Impact of *Eucalyptus nitens* and *Pinus radiata* fiber properties on the production process of lignocellulose nanofibrils

Gregory Albornoz-Palma[1,2,*], Sergio Henríquez-Gallegos[3], Isidora Ortega-Sanhueza[3], Roberto Teruel-Juanes[2], Amparo Ribes-Greus[2], Miguel Pereira[1,4]

[1]*Departamento de Ingeniería Química, Universidad de Concepción, Concepción, Chile.*
[2]*Instituto de Tecnología de Materiales (ITM), Universitat Politècnica de València (UPV), 46022 València, España.*
[3]*Facultad de Ciencias Forestales, Universidad de Concepción, Concepción, Chile.*
[4]*Centro de Excelencia en Nanotecnología (CEN), Román Díaz 532, Providencia, Santiago 7500000, Chile.*

Abstract

Lignocellulose nanofibrils (LCNFs) are nano-objects produced from different sources of lignocellulosic biomass. The physical and chemical properties of the plant cells that make up the raw material are diverse and affect the qualities of the LCNFs. Due to their chemical differences, understanding the effect that the physical properties of the raw material confer on LCNFs is complex. This study aims at comprehending the impact that the physical properties and the chemical composition of the raw materials from *Pinus radiata* and *Eucalyptus nitens* have on the mechanical processes of fibrillation and the final properties of LCNFs. The anatomical, physical, and component differences of the fibers in the different fractions and species showed a non-effect on the longitudinal disintegration during the mechanical processes of fibrillation. In addition, the LCNFs produced from smaller fibers showed a smaller average width, with *Eucalyptus nitens* being the species that had smaller and more homogeneous nanofibrils. Nevertheless, the organization of the components (hemicellulose) from *Pinus radiata* on the surface of the fibrils, generates very hydrated and large fibrils and flocs, increasing the viscosities of the LCNF suspensions. A model was established between the intrinsic viscosity and aspect ratio of LCNFs ($\rho[\eta] = 0.15p^{1.68}$) and delignified CNFs ($\rho[\eta] = 0.031p^{1.94}$) that are independent of the pretreatments and the flexibility of the fibrils. Finally, the glass transition temperatures of lignin were not affected by physical changes in the raw material.

Keywords: Pinus radiata, *Eucalyptus nitens*, lignocellulose nanofibers, morphology, rheology

1. Introduction

The anatomical differences between the *Pinus radiata* D. Don and *Eucalyptus nitens* Maiden wood are well known (Sixta, 2006; Ek, 2009). Such differences originate mainly from the biological nature of the different species and their genetic and growth conditions (Ek, 2009). The types of plant cells that make up pine wood (tracheids, parenchyma, and epithelial cells) are less and more uniform than the plant cells of eucalyptus wood (vessels, libriform fiber, fiber tracheids, longitudinal and ray parenchyma). In addition, the plant cells of both species have differentiated morphology, e.g., Pine fibers (tracheids) are longer, thicker-walled, less flexible, and more resistant than eucalyptus fibers, which are smaller, thinner, and have smaller fibrillar angles (Melo, 1995; Donaldson, 2008; de Assis, 2019). The anatomical and morphological differences of plant cells can influence the production and characteristics of lignocellulosic nanomaterials.

Lignocellulose nanofibrils (LCNFs) are nano-objects with widths lower than 100 nm, produced from the cell walls of plant cells of wood and plants by mechanical fibrillation processes in an aqueous medium (Chirayil, 2014; Oliaei, 2021). LCNFs have lengths of several micrometers, so

their aspect ratio is in the order of hundreds (Albornoz-Palma, 2020b). LCNFs have great potential for uses; they are more ecological and cheaper to produce than delignified CNFs (Delgado-Aguilar, 2015; Rojo, 2015; Zhang, 2022).

LCNFs are semi-flexible fibrils that generate viscous suspensions due to the hygroscopic nature of the cellulose and hemicellulose, the high aspect ratio, and the high specific surface area of the nanofibrils, causing strong interconnections at low concentrations (Nechyporchuk, 2016). At low concentrations of fibrils (dilute region), the interaction effects between them are insignificant, and the suspensions behave as Newtonian fluids (Iwamoto, 2014). However, above the critical concentration (Krishnan, 2010), the fibrils begin to interact, forming flocs and entangles, and suspensions behave as Pseudoplastic fluids (Saarrinen, 2009; Lê, 2018).

The differences in the viscosities of the fibrils depend on the physical and chemical characteristics of the fibrils, whose features are given by the raw material and the production processes of LCNFs.

The role of the physical properties of the plant cells of raw material in the production of LCNFs is still unclear, as there is some controversy regarding its importance and the variables that affect the production processes of LCNFs (Espinosa, 2017a; Espinosa, 2017b). In several studies, it has been shown that the morphology of the fibers of the raw material, crystallinity index, and the degree of polymerization have a degree of influence on the fibrillation process (Stelte, 2009; Besbes, 2011; Wang, 2015; Qin, 2016; Henríquez-Gallegos, 2021), the characteristics of the LCNFs, the mechanical properties, and reinforcement capability (Zimermann, 2004; Henriksson, 2008; Stelte, 2009). For this reason, this study seeks to understand the effect of the physical properties of fibers from *Pinus radiata* and *Eucalyptus nitens,* and their components, on the mechanical production process and the morphological and rheological characteristics of LCNFs.

2. Materials and methods

Materials: Wood chips from *Pinus radiata* and *Eucalyptus nitens* were used. The wood chips were fibrillated in a Bauer Bros Co. Model 148-2 disc refiner. The pulp of each species was fractionated by size in water using a Bauer-McNett classifier with 28, 48, and 100 mesh. The classification was carried out for 30 min, with constant water flow and agitation, obtaining four pulps with different fiber sizes. The pulps were named indicating the species and the fraction of the fibers retained in the mesh (Pinus-28, Pinus-48, Pinus-100, Pinus-under 100, Eucalyptus-28, Eucalyptus-48, Eucalyptus-100, and Eucalyptus-under 100).

Chemical compositions of fibers: The polymeric components of the fibers were quantified according to the methodology mentioned in Andrade et al. (2021). The extractives and ash were quantified according to T 204 cm-97 (with acetone as solvent) and T 211 cm-9, respectively.

Morphology of fibers: An L&W fiber analyzer was used to quantify the morphological parameters of the fibers. Fiber suspensions of 0.4% (w/w) consistency were used for the measurements. All measurements were performed in triplicate.

Degree of polymerization (DP): Bleached pulp with acid chlorite was used for measurements of the degree of polymerization (DP) of the cellulose. Measurements were made according to the methodology shown in Chakraborty et al. (2006) with cupriethylenediamine (CED) as solvent.

The crystallinity index (CrI): The pulps were freeze-dried. 50 mg freeze-dried pulp was pressed to form pellets. The pellets were analyzed by X-ray Diffraction (XRD) in a D4 Endeavor X-ray diffractometer (Bruker AXS Gmbh, Karlsruhe, Germany) with monochromatic Cu Kα radiation ($\lambda = 0.154$ nm) at 40 kV and 20 mA, in a 2θ range between 5° and 45°, with scan steps of 0.02°. The crystallinity index (CrI) was calculated according to Segal et al. (1959), using the Equation 1:

$$\mathrm{CrI} = \frac{I_{200} - I_{am}}{I_{200}} \quad (1)$$

where I_{200} is the maximum intensity of the (200) reflection (22.3° 2θ), and I_{am} is the minimum in the diffraction intensity associated with the intensity of the amorphous fraction (18.5° 2θ).

Production of LCNF suspensions: For the production of LCNFs, the pulps were refined with 50,000 revs in a PFI No 205 mill at a consistency of 10% (w/w) and homogenized in a Panda Plus 2000 homogenizer (GEA Niro Soavi) at a pressure of 700 bar, 0.5% (w/w), and 0, 5, 10, and 15 passes.

Morphological characteristics of the LCNFs: Apparent length distributions of the fibrils in the LCNF suspensions were measured in an S3500 Laser Diffraction Particle Size Analyzer (Microtrac Inc. USA) with a lignin refractive index of 1.61 (Li et al. 2018).

The average width of the LCNFs with 0, 5, and 10 passes through the homogenizer was determined by micrographs of Transmission Electron Microscopy (TEM) (JEM 1200EX-II JEOL) quantifying 240 fibrils. For LCNFs with 15 passes, width distributions were determined by quantifying 1000 fibril widths using TEM micrographs (Hitachi TEM). ImageJ software was used for processing the TEM images.

The aspect ratio of the LCNFs was calculated by dividing the average apparent length and the average width of fibrils.

The radius of gyration and the flexibility parameter (ε) of LCNFs were determined using the wormlike chain model (Mansfield, 2008) with the experimental values of average apparent lengths and widths, and intrinsic viscosity.

The viscosity of LCNF suspensions: The viscosities of the LCNF suspensions were measured in a rotational viscometer (Fungilab Premium-L, USA) in the concentration range from 0.02 to 0.5% (g/ml). Measurements were made at 25°C and 73.38 s^{-1}. The intrinsic viscosity was determined using the viscosity values below the critical concentration according to the methodology of Albornoz-Palma et al. (2020a).

Lignin nanoparticles: The determination of the quantity and chemical characterization of the lignin nanoparticles was carried out according to Albornoz-Palma et al. (2022b).

ζ-potential of LCNF suspension: Particle Metrix equipment (Stabino) was used to measure the ζ-potential of LCNFs in suspensions of 0.05% (w/w) consistency. The method used was the Transmission Potential method.

Formation of nanopapers: The LCNF suspensions at 0.5% (w/w) were concentrated to 15% (w/w) by vacuum filtration, using 0.45 µm pore diameter membranes. Subsequently, these suspensions were filtered in a Buchner funnel with a 6 cm diameter fritted disk, producing nanopapers with a grammage of 800 g/m^2. The nanopapers were pressed and dried in a vacuum oven for 7 days.

Fourier-Transform Infrared Spectroscopy (FTIR): FTIR spectroscopy measurements were performed on the dried nanopapers. An Agilent Cary 630 FTIR spectrometer (Mettler Toledo, USA) in the attenuated total reflectance mode (ATR) was used. The spectra were measured in the wavelength range from 4000 to 500 cm^{-1} with a 4 cm^{-1} resolution and an average of 64 scans. Spectra were area normalized and compared (principal component analysis) in The Unscrambler X program.

Thermogravimetric analysis (TGA): To determine the mass losses due to the thermal decomposition of the fibrils, a TGA 851 analyzer (Mettler Toledo, USA) was used. Samples of 3 to 5 mg were introduced into 70 µL alumina capsules. The temperature range was from 25°C to 600°C at a rate of 10°C/min in an oxidative atmosphere (50 mL/min).

Differential Scanning Calorimetry (DSC): Calorimetry analysis in a DSC 822e (Mettler Toledo, USA) was performed on the nanopapers to determine the glass transition temperatures of lignin and the difference in heat capacities. Samples of 3 and 5 mg were placed in 40 µL aluminum crucibles. The analysis method consisted of different consecutive heating/cooling/heating segments between -10°C and 200°C with a heating/cooling rate of 10°C/min. The tests were carried out under an inert atmosphere of N_2 at 50 mL/min flow.

Data analysis: The statistical analysis of the data was performed with the Statgraphics Centurion XVIII program.

3. Results and discussion

Pulp characterization: The fractionation by the size of the mechanical pulps of *Pinus radiata* and Eucalyptus *nitens* generated raw materials with different physical characteristics.

Table 1 shows that the plant cells of both *Pinus radiata* and *Eucalyptus nitens* presented lower average lengths and average diameters for the fractions obtained with finer meshes. The mechanical refining process used to produce raw materials generates the disintegration of wood chips through shear forces, producing a heterogeneous material in size made up of aggregates of fibers, fibers, and fines. The smallest fibers in the higher mesh fractions were significantly damaged in their structure, showing a lower degree of polymerization and crystallinity index. The latter parameter only had significant changes (with 95% confidence) between the fractions 100 and under 100 for *Eucalyptus nitens* and the fraction under 100 for *Pinus radiata*.

The percentage of fines had higher in the smaller size fraction due to their reduced dimensions, mainly fiber fragments and smaller plant cells. However, in 28 mesh fractions, the percentage of fines increases because the larger fibers tend to become entangled, favoring the retention of smaller structures.

Table 1. Morphological characteristics of *Eucalyptus nitens* and *Pinus radiata* pulps.

Properties	Average length (mm)	Variation of length [(a)] (%)	Average diameter (μm)	Variation of diameter[(a)] (%)	Crystallinity index[(b)] (%)	Variation of crystallinity index[(a)] (%)	Fines (%)	Degree of polymerization	Variation of degree of polymerization [(a)] (%)	Coarseness (mg/100m)
Pinus-28	2.03±0.06	-	44.1±0.2	-	67.4±0.6	-	32.7±0.6	1720	-	1.322±0.008
Pinus-48	1.11±0.04	45	41.7±0.3	5%	66.1±0.7	2%	19.1±3.2	1337	22%	0.724±0.007
Pinus-100	0.53±0.02	74	33.1±0.5	25%	62.0±1.5	8%	28.1±3.9	1302	24%	0.335±0.018
Pinus-under 100	0.27±0.01	87	29.9±0.6	32%	53.5±1.0	21%	69.5±0.8	1102	36%	0.148±0.009
Eucalyptus-28	1.37±0.05	-	41.2±0.1	-	64.9±0.2	-	48.3±0.8	1643	-	9.705±0.010
Eucalyptus-48	0.89±0.05	35	35.9±0.1	13%	64.3±0.3	1%	28.4±0.1	1470	11%	1.543±0.055
Eucalyptus-100	0.51±0.03	63	29.1±0.1	29%	63.6±0.8	2%	30.2±1.8	1354	18%	0.464±0.02
Eucalyptus-under 100	0.24±0.01	82	22.9±0.1	44%	57.0±0.7	12%	69.0±0.7	1187	28%	0.118±0.017

[(a)]Normalized respect to 28 mesh

[(b)]XRD diffractograms are shown in Figure S1 and Figure S2 (Supplementary material)

Until now, there has been talked about the physical changes of the fibers that component the different fractions. However, anatomical aspects of plant cells and their effects have not been considered. The plant cells that make up pine pulp are simple than those of eucalyptus because they have a limited and more uniform number of cell types. The xylem of softwoods (e.g., *Pinus radiata*) is mainly made up of tracheids (2-3 mm in length and 30 µm in diameter approximately (Donaldson, 2016)) and, to a lesser extent by, parenchyma and epithelial cells. On the other hand, the xylem of hardwoods (e.g., *Eucalyptus nitens*) is mainly made up of vessels, fibers (libriform fibers and fiber tracheids) (0.7-1.6 mm in length and 20 µm in diameter approximately (Elmas, 2018; Morais, 2019)), and to a lesser extent by parenchyma (longitudinal and ray cells) (Ek, 2009). The anatomical differences between the different structures produce differences in the refining process, with the parenchyma being the easiest to fibrillate, due to its thin-walled and smaller size (Ek, 2009; Wang, 2015), predominantly found in the smaller size fractions.

When comparing the variation in diameter between both species (Table 1), it is observed that it is higher for *Eucalyptus nitens*. As mentioned above, the plant cells in the eucalyptus pulps are more diverse, with the fibers found in higher proportions in the larger fractions. This is observed in

the high coarseness values for fraction 28, which is associated with density and cell wall thickness, being higher in libriform and tracheid fibers (Ek, 2009; Carrillo, 2015; Morais, 2019).

The variations of the length, crystallinity index, and degree of polymerization were higher for pine pulp, due to the more aggressive refining process required to produce the pulps. For simplicity, the term fibers is used to refer to all anatomical structures of the pulps (plant cells), regardless of species.

The characterization of the main components in the pulps of *Pinus radiata* is shown in Figure 1a. The percentage of cellulose, hemicellulose, and lignin does not change significantly in the 28, 48, and 100 mesh fractions. However, in the under 100 mesh fraction, the percentage of lignin increases, and cellulose decreases. The extractives were 0.97±0.01% for all fractions. The ashes were 0.25±0.01, 0.51±0.01, 0.71±0.01, and 2.1±0.1% for the 28, 48, 100, and under 100 mesh fractions respectively. On the other hand, Eucalyptus nitens pulps (Figure 1b) showed an increase in the percentage of lignin between the 28 and 48 mesh fractions (with no significant differences in the smaller size fractions) and a decrease in the percentage of cellulose. The 100 and under 100 fractions showed a reduction in the percentage of hemicellulose. The extractives were 0.96±0.02% for all fractions. The ashes were 0.28±0.01, 0.20±0.01, 0.19±0.01, and 1.2±0.1% for the 28, 48, 100, and under 100 mesh fractions respectively.

LCNF characterization: The production of LCNFs is affected by the characteristics of the raw material used (Stelte, 2009; Besbes, 2011; Wang, 2015). The surface chemical changes of the LCNFs with 15 passes through the homogenizer were studied using FTIR-ATR absorption spectra shown in Figure 1c-d. The LCNFs produced from pine pulp (Figure 1c) show slight differences in the absorbance of specific peaks between the different fractions. Peaks at 1158, 1105, 1050, and 1026 cm^{-1} showed a lower absorbance for 48 and under 100 fractions. These peaks are associated with the C–O stretching of the ether group and vibrations of C─O bonds in primary and secondary alcohol groups (Bykov, 2008; Lehto, 2018). This decrease in the peaks indicates a lower presence of the β-O-4 ether bonds in the lignin, generated by the severe mechanical process applied to the fibers that produced its rupture.

For the LCNFs from *Eucalyptus nitens* pulps, a higher number of differences in the absorption peaks were observed between the fibrils of the 28 mesh fraction and the other fractions. Peaks 1730 (C=O stretching of the unconjugated ketone, carboxyl, and ester group (Stark, 2016), 1459 (CH2 deformation stretching in lignin and xylan (Lehto, 2018)), 1333 (aryl ring breathing with C–O stretch (Stark, 2016)), 1234 (C–O stretching of the ether group (Lehto, 2018)), 1105, 1051, and 1031 cm^{-1} (C─O bonds in primary and secondary alcohol) show a lower absorbance for the LCNFs from 48, 100, and under 100 mesh fractions. This indicates that the lignin in the LCNFs of these fractions has a greater presence on the surface of the fibrils, a lower degree of oxidation, and a lower amount of β-O-4 ether bonds.

To understand the changes in fibrils during the production process of LCNFs, due to the physical characteristics of the fibers in the raw materials, their characteristics of the fibrils have been determined at different stages of the production process, the results of which are shown in Table 2.

The mechanical refining pretreatment generates a decrease in the average widths and apparent lengths of the fibrils (0 passes) produced from raw materials with a smaller fiber morphology. However, when analyzing the variations of width, no changes are observed between the fractions of the different species or between the species. The decrease in the average diameters and the constant values in the variation of width of the fibrils indicate that the anatomical, physical, and chemical differences of the fibers in the raw materials do not have an effect on the longitudinal disintegration during the refining process, but they generate differences in the characteristics of LCNFs.

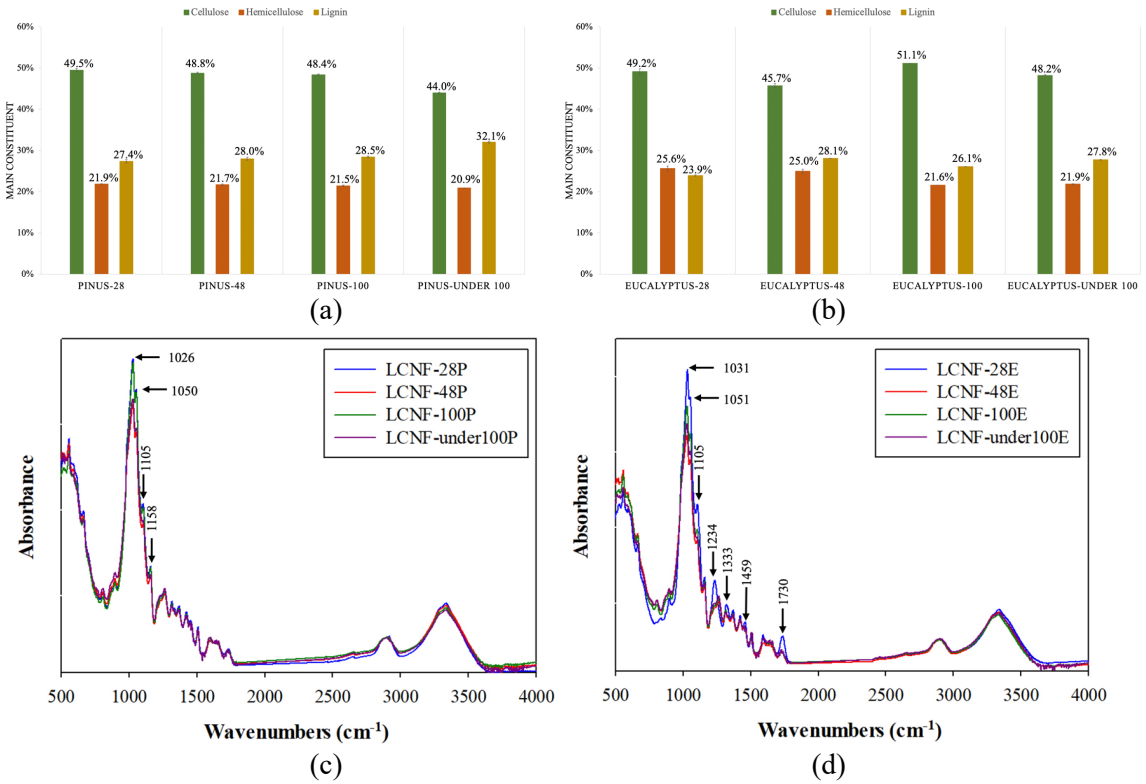

Figure 1. (a) Chemical composition of mechanical *Pinus radiata* pulps, (b) chemical composition of mechanical *Eucalyptus nitens* pulps, (c) FTIR-ATR spectrum of LCNFs from *Pinus radiata* pulp, and (d) LCNFs from *Eucalyptus nitens* pulp.

Average lengths don't show an important difference between the 28, 48, and 100 mesh fractions, and decrease for the under 100 mesh fraction, in both species (Table 2). The variation of apparent length decreases with the decrease in the size of the fibrils in the raw material. Refining is a disintegration process of the fibers using shear forces, which affects larger fibers in greater proportion, generating their rupture.

To analyze the effect that the mechanical process of homogenization has on the average width, and apparent length of the fibrils with different numbers of passes (5, 10, and 15 passes, Table 2), a decrease in these parameters is observed, whose variation increases and is higher for the width. This is because the homogenization process produces the disintegration of the fibrils using the mechanism of impact and shear force mainly (surface mechanisms) (Lee, 2014; Costa, 2018), which favors longitudinal disintegration, increasing the aspect ratio.

However, when comparing the variation of apparent lengths and widths of the different LCNFs by species, no important differences are observed, except the LCNFs of *Pinus radiata* of the under 100 mesh fraction with 10 and 15 passes, whose variations of apparent length decreased. This non-change in values of variations indicates that the morphological, chemical, and anatomical differences of the fibers of the raw materials don´t have a significant effect on fibrillation by homogenization. LCNFs of Pinus radiata show a higher variation of apparent lengths, caused by the lower coarseness, which favors their rupture.

The aspect ratio increased with the number of passes through the homogenizer (Table 2) because the homogenization process predominantly generates longitudinal disintegration over transverse disintegration. The decrease in the size of the fibrils due to homogenization produces an increase in the fibrillar population per unit mass, causing an increase in the hydrodynamic volume of

the fibrils in the suspensions, which is reflected in an increase in the resistance to flow and intrinsic viscosity.

Chemical differences in the raw materials can generate differences in the surface charges of the fibrils, affecting the production process and the characteristics of the LCNFs. Although the FTIR-ATR spectra showed an increase in the oxidized groups in the LCNF from *Eucalyptus nitens* and the 28 mesh fraction, ζ-potentials of fibrils do not change significantly between the LCNFs of different fractions and the number of passes through the homogenizer (Figure 1d and Table 2). The LCNFs of *Eucalyptus nitens* showed a slightly higher ζ-potential (absolute value) caused by the higher presence of hemicellulose (uronic acids) (Nechyporchuk, 2016).

Table 2. Morphological characterization of LCNFs with different numbers of passes through the homogenizer and lignin content.

Raw materials	Passes	Average Width (nm)	Variation of width[a] (%)	Apparent average length (*μm*)	Variation of apparent length[c] (%)	Aspect ratio	Intrinsic viscosity (ml/g)	ζ-potential[d]	Lignin nanoparticle[e] (% g/g)
Pinus-28	0	197.3	99.6[b]	12.6	99.4[b]	64	96	-21.0	1.6
	5	120.6	39	8.9	29	74	151	-19.8	1.6
	10	88.1	55	7.3	42	83	173	-19.3	1.7
	15	51.8	74	6.2	51	120	281	-19.1	1.9
Pinus-48	0	166.2	99.6[b]	12.4	98.9[b]	75	145	-20.5	1.5
	5	93.5	44	8.9	28	95	206	-20.3	1.5
	10	76.7	54	7.3	41	95	220	-20.1	1.5
	15	50.4	70	6.2	50	123	300	-20.0	1.6
Pinus-100	0	140.3	99.6[b]	12.5	97.6[b]	89	183	-20.9	1.2
	5	89.5	36	8.8	30	98	219	-20.4	1.5
	10	61.8	56	7.3	42	118	290	-20.2	1.5
	15	48.5	66	6.2	50	128	326	-20.1	2.4
Pinus-under 100	0	110.2	99.6[b]	9.1	96.6[b]	83	167	-20.8	1.3
	5	66.1	40	7.4	19	112	279	-19.7	1.4
	10	53.1	52	6.3	31	119	296	-19.4	1.5
	15	38.3	65	5.3	42	138	349	-19.4	2.3
Eucalyptus-28	0	145.8	99.6[b]	8.8	99.4[b]	60	109	-23.3	2.0
	5	92.4	37	7.6	14	82	156	-22.6	2.1
	10	67.1	54	6.4	27	95	194	-22.1	2.1
	15	48.5	67	5.5	38	113	273	-24.0	2.6
Eucalyptus-48	0	132.1	99.6[b]	8.5	99.0[b]	64	122	-23.6	1.8
	5	88.7	33	7.6	11	86	175	-22.6	2.3
	10	58.1	56	6.4	25	110	266	-22.6	2.3
	15	46.2	65	5.5	35	119	293	-22.9	2.6
Eucalyptus-100	0	114.7	99.6[b]	8.4	98.4[b]	73	134	-23.0	1.6
	5	81.5	29	7.6	10	93	203	-22.8	1.8
	10	52.7	54	6.5	23	123	297	-22.3	3.0
	15	39.1	65	5.3	37	136	333	-23.0	3.1
Eucalyptus-under 100	0	88.9	99.6[b]	7.5	96.9[b]	84	173	-23.7	1.9
	5	54.4	39	6.3	16	116	295	-23.0	2.1
	10	41.3	54	5.4	28	131	338	-22.6	3.2
	15	32.8	63	4.7	37	143	380	-22.2	3.5

[a] Normalized to the average width of 0 passes through the homogenizer for each raw material.
[b] Normalized to the parameters of raw materials
[c] Normalized to the apparent average length of 0 passes through the homogenizer for each raw material
[d] pH of 4.9 ± 0.3
[e] Based on total lignin.

The mechanical processes of fibrillation produce removing part of the lignin from the fibrils, forming lignin nanoparticles (Jiang, 2018). Lignin nanoparticles are spherical form structures found in suspension or between the fibrils (ζ-potential = -0.1 ± 0.1 mV). Table 2 shows that the amount of lignin nanoparticles formed is low (lower than 3.5% of the total lignin of the fibrils), being slightly higher for the LCNFs from *Eucalyptus nitens*. The lignin in eucalyptus fibrils has a higher proportion of S-type lignin (Rencoret, 2007; Antes, 2015). S-type lignin is more reactive and less crosslinked than G-type lignin (Muraleedharan, 2018), which facilitates its removal.

Finally, it can be established that both the mechanical processes of refining and homogenization are not affected by the morphology, structure, and anatomy of the fibers of the raw materials of each species. However, slight differences between species were observed, where transverse disintegration and ζ-potential were lower for LCNFs from *Eucalyptus nitens*.

LCNF characteristics with 15 passes through the homogenizer: To analyze the effect of the physical characteristics of the raw materials on the features of the LCNFs, more detailed measurements of the morphology of the LCNFs with 15 passes through the homogenizer were made, whose distributions are shown in Figure 2 and Figure 3. The quantification of the distribution parameters is shown in Table 3.

Width distributions shown in Figure 2 for the LCNFs from *Pinus radiata* and *Eucalyptus nitens* show a displacement in the distributions to smaller width values for the LCNFs produced from the smallest size fibers. This displacement is reflected in the increase in nanofibrillar yield (fibrils with diameters lower than 100 nm). For LCNFs from *Pinus radiata*, the nanofibrillar yield increased from 93% for LCNF-28P to 94, 96, and 98% for LCNF-48P, LCNF-100P, and LCNF-under100P, respectively. For LCNFs from *Eucalyptus nitens*, the nanofibrillar yield increased from 90% for LCNF-28E to 91, 92, and 95% for LCNF-48E, LCNF-100E, and LCNF-under100E, respectively. Table 3 shows that the average widths decrease for the LCNFs produced from the smaller size fibers (for both species), without significant changes in the coefficient of variation, except for LCNF-28P. These results indicate that the LCNFs produced from smaller fibers are thinner but without changes in homogeneity. *Eucalyptus nitens* is the species that has a more homogeneous nanomaterial in width for the same production process.

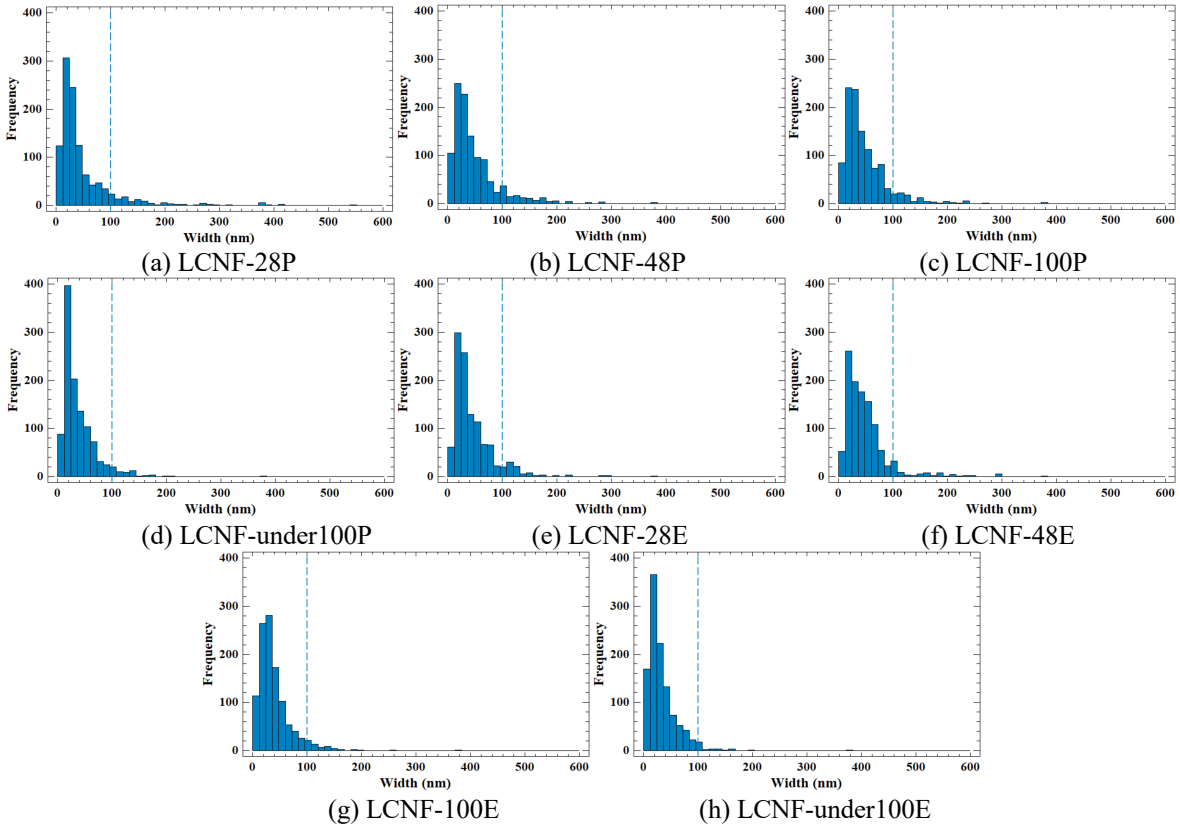

Figure 2. Width distributions of LCNFs from *Pinus radiata* and *Eucalyptus nitens* pulps.

The average width of the LCNFs of the *Eucalyptus nitens* pulps is directly related (linear relationship) to the average diameter of the fibers of its raw material, with a correlation coefficient (*r*) of 0.99. For the LCNFs of *Pinus radiata*, the average width is linearly related to the crystallinity index of the raw material, with an r = 0.98 (correlation coefficient). The other variables (degree of polymerization and coarseness) of the raw materials are not directly related to the average width of the LCNFs.

Figure 3 shows the apparent length distributions. These distributions show non-change between fractions, for each species, except for LCNF-under100E. When quantifying the parameters that characterize the distributions (Table 3), it is observed that the average apparent lengths and the coefficient of variation of the distributions non-change significantly between the 28, 48, and 100 mesh fractions for LCNFs from *Pinus radiata*, and the 28 and 48 mesh fractions for LCNFs from *Eucalyptus nitens*. These results show that the production process of LCNFs affects to a greater extent the transverse disintegration of the larger fibers, producing nanomaterials of equal or smaller lengths but without changes in the homogeneity of the apparent lengths, regardless of the specie.

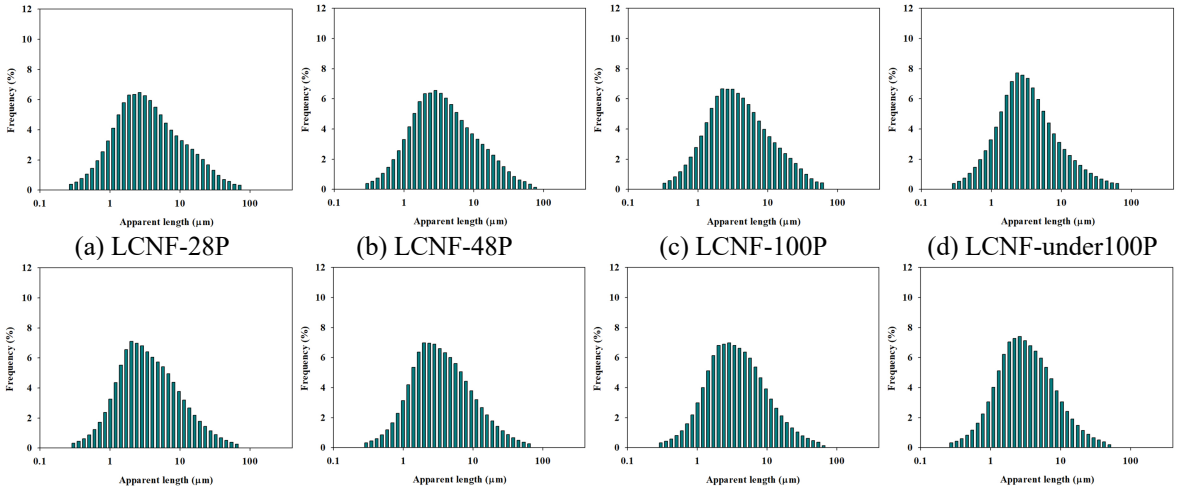

(a) LCNF-28P (b) LCNF-48P (c) LCNF-100P (d) LCNF-under100P

(e) LCNF-28E (f) LCNF-48E (g) LCNF-100E (h) LCNF-under100E

Figure 3. Apparent length distributions of LCNFs from *Pinus radiata* and *Eucalyptus nitens* pulps.

Viscosity data as a function of concentration is shown in Figure 4. For LCNFs from *Pinus radiata*, it is observed that the viscosity does not change between the 28, 48, and 100 mesh fractions, and increases slightly for the under 100 mesh fraction. This increase is observed in the semi-dilute region, above the critical concentration (Table 3). The interactions between the fibrils are significant, and flocs have been generated that increase the resistance to flow (Saarrinen, 2009). The flocs depend on the size of the fibrils and their surface charge. Table 2 and Table 3 show that the ζ-potential of the LCNFs does not change between the fractions and the radius of gyration of the fibrils decreases only for the under 100 mesh fraction. This decrease indicates an increase in the fibrillar population per unit mass, generating larger flocs, which increase resistance to flow. For LCNFs from *Eucalyptus nitens*, a progressive increase in viscosity is observed for the LCNFs produced from the smaller size fractions. This trend is due to the decrease in the size of the fibrils, observed in a reduction in the radius of gyration (Table 3), which produces an increase in the fibrillar population, generating larger flocs.

Table 3. Morphological and rheological characterization of LCNFs from *Pinus radiata* and *Eucalyptus nitens* with 15 passes through the homogenizer.

Sample	Average width (*nm*)	S.D. of the sample [(a)] (*nm*)/Coefficient of variation (%)	Average apparent length (*μm*)	S.D. of the sample (*μm*)/Coefficient of variation (%)	Radius of gyration[(b)] (*μm*)	Critical concentration (mg/ml)
LCNF-28P	51.8±0.8	21.8/42	6.2±0.1	2.83/46	1.53	3.33
LCNF-48P	50.4±0.3	16.4/33	6.2±0.2	2.86/46	1.53	2.68
LCNF-100P	48.5±0.7	14.5/30	6.2±0.1	2.81/45	1.53	2.50
LCNF-under100P	38.3±0.6	11.4/30	5.3±0.3	2.44/46	1.30	2.13
LCNF-28E	48.5±0.3	13.8/28	5.5±0.1	2.76/50	1.36	3.66
LCNF-48E	46.2±0.7	12.5/27	5.5±0.4	2.76/50	1.35	2.58
LCNF-100E	39.1±0.5	10.4/27	5.3±0.2	2.76/52	1.30	2.14
LCNF-under100E	32.8±0.6	8.7/27	4.7±0.2	2.70/57	1.15	2.08

[(a)]Normal distribution by the central limit theorem.
[(b)]Wormlike chain model (Mansfield, 2008)

Figure 4 shows that the viscosities of suspensions of LCNFs from *Pinus radiata* are higher than those of LCNFs from *Eucalyptus nitens*. The difference between the viscosities cannot be explained by the size of the fibrils, because the LCNF-under100P and LCNF-100E have the same average apparent lengths and widths. This difference could be due to the organization of the components on the surface of the LCNFs, where pine fibrils would be surrounded by hemicellulose, unlike eucalyptus fibrils, where glucomannans would be partially exposed (Kumagai, 2018; Tarasov, 2018). LCNFs from *Eucalyptus nitens* have a slightly higher ζ-potential than LCNFs from *Pinus radiata* (Table 2). This could be due to the higher amount of exposed hydroxyl groups of the cellulose on its surface. In addition, hemicellulose is a polymer more hygroscopic than cellulose, so it attracts a greater amount of water molecules due to its branched structure (Correia, 2017), which produces highly hydrated and large fibrils and flocs, generating an increase in resistance to flow.

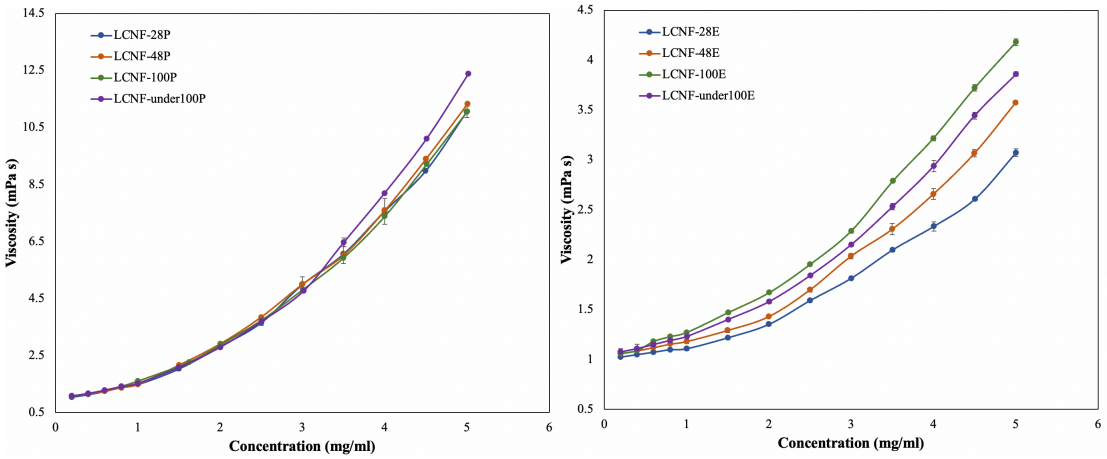

(a) (b)

Figure 4. Viscosities of LCNFs from (a) *Pinus radiata* and (b) *Eucalyptus nitens* pulps.

There is a power law relationship between morphological characteristics, expressed by aspect ratio (*p*), and rheological properties, by intrinsic viscosity ([η]), for cellulose nanomaterials (Tanaka, 2015; Albornoz-Palma, 2020a; Bastida, 2022). When studying this relationship for LCNFs with different production processes and raw materials (mechanical LCNFs, shown in this work; chemical

LCNFs (oxidized with acid chlorite, Table S1 Supplementary material); and enzymatic LCNFs (Albornoz-Palma, 2022b) from pine and eucalyptus pulps) the following expression was obtained:

$$\rho[\eta] = 0.15p^{1.68} \quad (1)$$

While when studying the relationship between delignified CNFs with different mechanical, enzymatic, and chemical treatments (Albornoz-Palma, 2020a; Albornoz-Palma, 2022a), the following expression was obtained:

$$\rho[\eta] = 0.031p^{1.94} \quad (2)$$

where ρ is the density of the LCNFs and delignified CNFs (ρ = 1.6 g/cm^3 (Daicho, 2019)).

Figure 5 shows the relationship between the experimental data and the models. The determination coefficients (R^2) are 99.4 and 98.5% for the LCNFs and delignified CNFs model, respectively, which shows that the models are suitable. These models allow related the dependence of the intrinsic viscosity to a single morphological variable, independent of the degree of flexibility of the fibrils and the species of the raw materials. In addition, they allow the determination of the average width of the fibrils (a complex variable) through two variables of quick and simple measurement (apparent length and intrinsic viscosity).

To compare the models of Albornoz-Palma et al. (2020a) ($\rho[\eta] = 0.051p^{1.85}$) and Equation 2, differences of lower than 2.6% and 4.9% in the prediction of the aspect ratio and intrinsic viscosity are obtained in the ranges studied ($\rho[\eta]$ entre 517 y 2144; y p entre 145 y 306). This slight difference is mainly due to incorporating new experimental data that allow the prediction range to be extended.

Figure 5 shows that the LCNFs have a higher intrinsic viscosity than the delignified CNFs, because the LCNFs are less flexible due to the cementing capacity of the lignin (Pandey, 1999; Albornoz-Palma, 2022b). This causes the fibrils to occupy a larger hydrodynamic volume per unit mass. As the aspect ratio increases, the differences between the intrinsic viscosities of delignified CNFs and LCNFs decrease, due to the elongated shape of the fibrils that allows higher flexibility and, therefore, a lower intrinsic viscosity. The changes in flexibility between high and low aspect ratio fibrils are much higher in LCNFs ($\varepsilon = 0.35 - 0.54$) than in delignified CNFs ($\varepsilon = 0.32$), resulting in a lower power index. The ε parameter is associated with the flexibility of the fibrils (Mansfield, 2008).

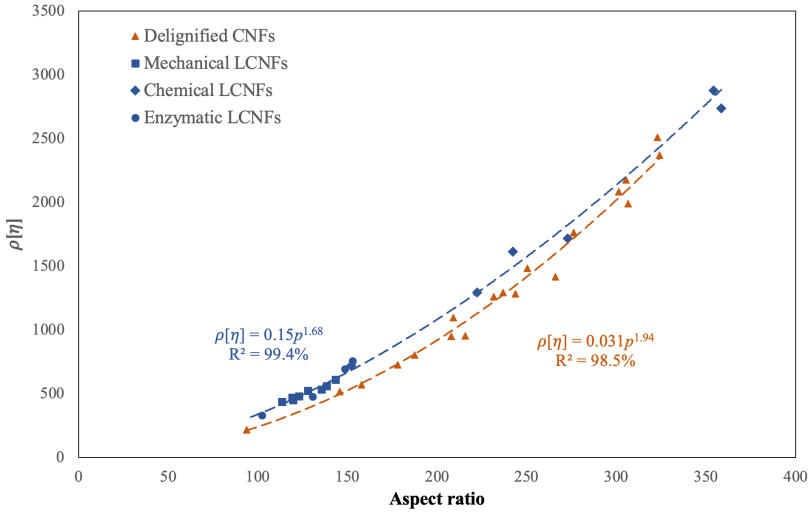

Figure 5. Relationship between intrinsic viscosity and aspect ratio of LCNFs and delignified CNFs.

Thermogravimetric and differential scanning calorimetry analysis of LCNFs. The differences in the components and their distribution in the LCNFs can generate differences in the water removal and thermal stability of these nanomaterials. Cellulose and hemicellulose have higher degradation rates than lignin. Cellulose begins its degradation around 315°C, hemicellulose at 190°C, and lignin at approximately 210°C (Yang, 2007; Dorez, 2014; Cao, 2019).

Figure 6 shows the TGA and DTG (Derivative Thermo Gravimetry) spectra of the different LCNFs. Three stages of mass loss are observed in the LCNFs of both species. The first stage (Peak 1) corresponds to the moisture loss of the LCNFs nanopapers. Despite the extensive drying process to which the nanopapers were subjected, they maintained a moisture percentage close to 5% due to the high hygroscopic capacity of cellulose and hemicellulose. The moisture in nanopapers of LCNFs from *Pinus radiata* is slightly higher than in nanopapers of LCNFs from *Eucalyptus nitens*. This is because glucomannans have a somewhat higher moisture adsorption capacity than xylans (Kulasinski, 2016), which generates higher water retention, increasing the onset and endset temperatures of evaporation (T_{onset} and T_{endset}).

In the second stage, the degradation onset temperature (T_{onset}) and the maximum degradation temperature ($T_{peak\ 2}$), mainly associated with the thermal decomposition of hemicellulose and lignin, do not show significant differences, regardless of the fraction and species.

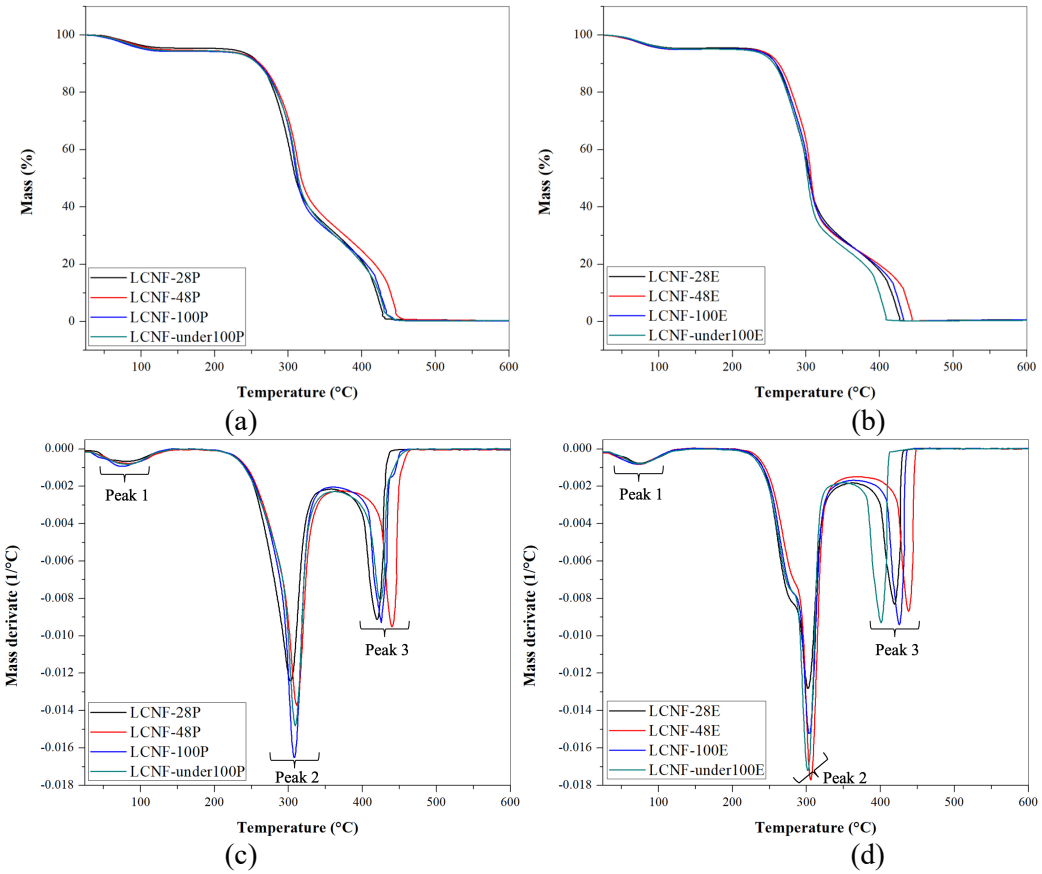

Figure 6. (a-b) TGA and (c-d) DTG spectra of LCNFs from *Pinus radiata* y *Eucalyptus nitens*.

The third stage (Peak 3) is mainly associated with cellulose and lignin degradation. The maximum degradation temperature ($T_{peak\ 3}$) is higher for the 48 mesh fraction and lower for the smaller size fractions in both species. This decrease could indicate a reduction in the degree of polymerization and crystallinity index in the fibrils produced from fibers with a lower value of these variables and

the same mechanical fibrillation process (Andrea Andrade, 2021; Albornoz-Palma, 2020a), which facilitates the thermal degradation of cellulose.

The glass transition temperature of lignin (Tg) was studied by DSC analysis in the temperature range from -10 to 200°C. Table 4 shows that the Tg values don´t change between the LCNFs of different fractions, for each species, except for the LCNF-28E, whose Tg value is lower. This decrease in Tg is explained by the higher degree of oxidation of lignin (Figure 1d), which facilitates its movement.

Finally, the increase in the difference in heat capacity (ΔCp) at Tg in the LCNFs-100P, LCNFs-under100P, and LCNFs-under100E indicates an increase in the crosslinking density of lignin (Heitner, 2019).

Table 4. Moisture and peaks of the thermal decomposition of LCNF nanopapers, and glass transition temperature and heat capacity difference of lignin in LCNFs from *Pinus radiata* and Eucalyptus *nitens*.

	Moisture			Degradation			Tg (°C)	ΔCp (J/gK)
Peak	Peak 1			-	Peak 2	Peak 3		
Sample	T_{onset} (°C)	T_{endset} (°C)	Moisture (%)	T_{onset} (°C)[(a)]	$T_{peak\ 2}$ (°C)	$T_{peak\ 3}$ (°C)		
LCNF-28P	52	109	4.6	259±1	303±1	419±1	98±1	0.165
LCNF-48P	54	107	5.0	263±1	311±1	437±1	99±1	0.112
LCNF-100P	50	107	4.9	263±1	308±2	428±2	98±1	0.298
LCNF-under100P	51	110	5.0	261±1	309±1	425±1	95±3	0.263
LCNF-28E	49	99	4.3	258±1	302±1	419±2	80±3	0.240
LCNF-48E	45	99	4.4	262±1	306±2	438±1	91±2	0.241
LCNF-100E	45	98	4.3	258±1	307±1	424±1	89±1	0.215
LCNF-under100E	47	104	4.2	257±1	304±2	402±1	89±2	0.271

[(a)]Corresponding to a degradation of 5%

4. Conclusions

The mechanical refining process produced a heterogeneous material in size, formed by aggregates of fibers, fibers, and fines. The smaller fibers in size showed greater damage in their structure, presenting a lower degree of polymerization, crystallinity index, and coarseness.

The anatomical, physical, and component differences of the fibers of the different size fractions did not show an effect on the longitudinal disintegration during the mechanical processes of refining and homogenization, in both species. However, an increase in transverse disintegration was shown during the mechanical refining process, being higher for LCNFs from *Eucalyptus nitens*. The homogenization process was not affected in the transverse disintegration of the fibers by the characteristics of the raw materials, being higher for the LCNFs of *Pinus radiata*.

The LCNFs produced from smaller fibers were thinner (lower width), but without changes in homogeneity, with *Eucalyptus nitens* being the species that had more homogeneous nanofibrils. On the other hand, the apparent length of the LCNFs was the same for the smaller mesh fractions (28 and 48 mesh), which showed that the mechanical processes affected larger fibers in greater proportion, without changes in homogeneity and regardless of the species. In addition, the LCNFs produced from *Eucalyptus nitens* pulp presented the fibrils with smaller sizes.

The viscosities of LCNF suspensions from *Pinus radiata* were higher than the viscosities of the LCNF suspensions from *Eucalyptus nitens*, which could be due to the organization of the

components on the surface of LCNFs, where the glucomannans are partially exposed on the surface of the fibrils of eucalyptus, generating very hydrated and large fibrils and flocs.

A power law model was established between a rheological parameter, intrinsic viscosity, and a morphological parameter, aspect ratio, for lignocellulose nanofibrils, independent of the pretreatments used during their production and of the flexibility of the fibrils.

Calorimetric analysis showed that the glass transition temperature of lignin was not affected by physical changes in the raw material and mechanical processes. Finally, the lignins in the fibrils produced from the higher mesh fractions showed increased crosslinks.

Ethics approval and consent to participate

Not applicable

Consent for publication

Not applicable

Availability of data and materials

Not applicable

Competing interests

The authors have no relevant financial or non-financial interests to disclose.

Funding

This work was funded by the Agencia Nacional de Investigación y Desarrollo (ANID)/Doctorado Nacional/2018–21181080, and projects FONDECYT N°1201042 and INNOMAT-H2 (MFA/2022/041) (Conselleria d'Innovació, Universitats, Ciència i Societat Digital).

Authors' contributions

Gregory Albornoz-Palma: Conceptualization, Methodology, Validation, Formal analysis, Investigation, Writing – Original Draft; **Isidora Ortega-Sanhueza:** Investigation; **Roberto Teruel-Juanes:** Methodology, Validation, Investigation; **Sergio Henríquez-Gallegos:** Investigation, Writing – Review & Editing; **Amparo Ribes-Greus:** Conceptualization, Validation, Resources, Writing – Review & Editing, Supervision; **Miguel Pereira:** Conceptualization, Validation, Resources, Writing – Review & Editing, Supervision, Funding acquisition.

Acknowledgments

We thank the Laboratorio de Biomateriales, Laboratorio de Análisis de Superficie y su Interacción con Fluidos (ASIF) (Departamento de Ingeniería Química, Universidad de Concepción).

Authors' information (optional)

Corresponding authors

E-mail: gralbornoz@udec.cl. Phone: +56412661169.

Reference

Albornoz-Palma G, Betancourt F, Mendonça RT, Chinga-Carrasco G, Pereira M (2020a) Relationship between rheological and morphological characteristics of cellulose nanofibrils in dilute dispersions. Carbohydr Polym 230:115588. https://doi.org/10.1016/j.carbpol.2019.115588

Albornoz-Palma G, Ching D, Andrade A, et al (2022a) Relationships between size distribution, morphological characteristics, and viscosity of cellulose nanofibril dispersions. Polymers (Basel) 14.18:3843 https://doi.org/10.3390/polym14183843

Albornoz-Palma G, Ching D, Henríquez-Gallegos S, et al (2022b) The role of lignin in the production process and characterization of lignocellulose nanofibril suspensions. Cellulose 29.16:8637-8650. https://doi.org/10.1007/s10570-022-04791-4

Albornoz-Palma G, Ching D, Valerio O, Mendonça RT, Pereira M (2020b) Effect of lignin and hemicellulose on the properties of lignocellulose nanofibril suspensions. Cellulose. https://doi.org/10.1007/s10570-020-03304-5

Andrade A, Henríquez-Gallegos S, Albornoz-Palma G, Pereira M (2021) Effect of the chemical and structural character- istics of pulps of Eucalyptus and Pinus on the deconstruc- tion of the cell wall during the production of cellulose nanofibrils. Cellulose 28(9):5387–5399. https://doi.org/10.1007/s10570-021-03848-0

Antes R, Joutsimo OP (2014) Effect of Modified Cooking on Chemical Composition of Pulps from Eucalyptus globulus and Eucalyptus nitens. Bioresources 10:. https://doi.org/10.15376/biores.10.1.210-226

Bastida GA, Schnell CN, Mocchiutti P, et al (2022) Effect of oxalic acid concentration and different mechanical pre-treatments on the production of cellulose micro/nanofibers. Nanomaterials (Basel) 12:2908. https://doi.org/10.3390/nano12172908

Besbes I, Vilar MR, Boufi S (2011) Nanofibrillated cellulose from Alfa, Eucalyptus and Pine fibres: Preparation, characteristics and reinforcing potential. Carbohydr Polym 86:1198–1206. https://doi.org/10.1016/j.carbpol.2011.06.015

Bykov, I. (2008). Characterization of natural and technical lignins using FTIR spectroscopy.

Cao W, Li J, Martí-Rosselló T, Zhang X (2019) Experimental study on the ignition characteristics of cellulose, hemicellulose, lignin and their mixtures. J Energy Inst 92:1303–1312. https://doi.org/10.1016/j.joei.2018.10.004

Carrillo, I., Aguayo, M. G., Valenzuela, S., Mendonça, R. T., & Elissetche, J. P. (2015). Variations in wood anatomy and fiber biometry of Eucalyptus globulus genotypes with different wood density. Wood research, *60*(1), 1-10.

Chakraborty A, Sain M, Kortschot M (2006) Reinforcing potential of wood pulp-derived microfibres in a PVA matrix. Holzforschung 60:53–58. https://doi.org/10.1515/hf.2006.010

Chirayil, C. J., Mathew, L., & Thomas, S. (2014) REVIEW OF RECENT RESEARCH IN NANO CELLULOSE PREPARATION FROM DIFFERENT LIGNOCELLULOSIC FIBERS. Rev Adv Mater Sci, *37*:20-28.

Correia VC, Santos SF, Savastano H Jr, John VM (2018) Utilization of vegetable fibers for production of reinforced cementitious materials. RILEM Tech Lett 2:145–154. https://doi.org/10.21809/rilemtechlett.2017.48

Costa ALR, Gomes A, Tibolla H, et al (2018) Cellulose nanofibers from banana peels as a Pickering emulsifier: High-energy emulsification processes. Carbohydr Polym 194:122–131. https://doi.org/10.1016/j.carbpol.2018.04.001

Daicho, K., Kobayashi, K., Fujisawa, S., & Saito, T. (2019). Crystallinity-independent yet modification-dependent true density of nanocellulose. Biomacromolecules, 21(2), 939-945.

de Assis, T., Pawlak, J., Pal, L., Jameel, H., Venditti, R., Reisinger, L. W., ... & Gonzalez, R. W. (2019) Comparison of wood and non-wood market pulps for tissue paper application. Bioresources, 14(3), 6781-6810.

Delgado Aguilar, M. (2015). Nanotecnología en el sector papelero: mejoras en calidad y permanencia de las fibras de alto rendimiento y secundarias en una economía circular mediante el uso de nanofibras y el refino enzimático. Tesis Doctoral. Universitat de Girona, España. https://dugi-doc.udg.edu/handle/10256/11737

Donaldson, L. (2008) Microfibril angle: measurement, variation and relationships–a review. Iawa Journal, 29(4), 345-386. https://doi.org/10.1163/22941932-90000192

Donaldson, L., Nanayakkara, B., Harrington, J. (2016) Wood Growth and Development. Encyclopedia of applied plant sciences, 2nd Edition, Vol. 1, Academic Press.

Dorez G, Ferry L, Sonnier R, et al (2014) Effect of cellulose, hemicellulose and lignin contents on pyrolysis and combustion of natural fibers. J Anal Appl Pyrolysis 107:323–331. https://doi.org/10.1016/j.jaap.2014.03.017

Ek M, Gellerstedt G, Henriksson G (eds) (2009) Pulp and paper chemistry and technology. Volume 1: Wood chemistry and wood biotechnology. Walter de Gruyter.

Elmas, G. M., Gürboy, B., & Eray, İ. N. (2018) Examining the pulp production compatibility of earlywood and latewood in Willow (Salix excelsa) clones in terms of fiber morphology. Bioresources, 13(4), 8555-8568.

Espinosa E, Sánchez R, Otero R, et al (2017b) A comparative study of the suitability of different cereal straws for lignocellulose nanofibers isolation. Int J Biol Macromol 103:990–999. https://doi.org/10.1016/j.ijbiomac.2017.05.156

Espinosa E, Sánchez R, González Z, et al (2017) Rapidly growing vegetables as new sources for lignocellulose nanofibre isolation: Physicochemical, thermal and rheological characterisation. Carbohydr Polym 175:27–37. https://doi.org/10.1016/j.carbpol.2017.07.055

Heitner C, Dimmel D, Schmidt J (eds) (2016) Lignin and Lignans: Advances in Chemistry. CRC Press, Boca Raton, FL

Henriksson M, Berglund LA, Isaksson P, et al (2008) Cellulose nanopaper structures of high toughness. Biomacromolecules 9:1579–1585. https://doi.org/10.1021/bm800038n

Henríquez-Gallegos S, Albornoz-Palma G, Andrade A, Soto C, Pereira M (2021) Impact of the enzyme charge on the production and morphological features of cellulose nanofibrils. Polymers 13(19):3238. https://doi.org/10.3390/polym13193238

Iwamoto S, Lee S-H, Endo T (2014) Relationship between aspect ratio and suspension viscosity of wood cellulose nanofibers. Polym J 46:73–76. https://doi.org/10.1038/pj.2013.64

Jiang Y, Liu X, Yang Q, et al (2018) Effects of residual lignin on mechanical defibrillation process of cellulosic fiber for producing lignocellulose nanofibrils. Cellulose 25:6479–6494. https://doi.org/10.1007/s10570-018-2042-6

Kulasinski K, Salmén L, Derome D, Carmeliet J (2016) Moisture adsorption of glucomannan and xylan hemicelluloses. Cellulose 23:1629–1637. https://doi.org/10.1007/s10570-016-0944-8

Kumagai A, Endo T (2018) Comparison of the surface constitutions of hemicelluloses on lignocellulosic nanofibers prepared from softwood and hardwood. Cellulose 25:3885–3897. https://doi.org/10.1007/s10570-018-1861-9

Lê HQ, Dimic-Misic K, Johansson L-S, et al (2018) Effect of lignin on the morphology and rheological properties of nanofibrillated cellulose produced from γ-valerolactone/water fractionation process. Cellulose 25:179–194. https://doi.org/10.1007/s10570-017-1602-5

Lee J-A, Yoon M-J, Lee E-S, et al (2014) Preparation and characterization of cellulose nanofibers (CNFs) from microcrystalline cellulose (MCC) and CNF/polyamide 6 composites. Macromol Res 22:738–745. https://doi.org/10.1007/s13233-014-2121-y

Lehto J, Louhelainen J, Kłosińska T, et al (2018) Characterization of alkali-extracted wood by FTIR-ATR spectroscopy. Biomass Convers Biorefin 8:847–855. https://doi.org/10.1007/s13399-018-0327-5

Li Y, Fu Q, Yang X, Berglund L (2018) Transparent wood for functional and structural applicationsPhilos. Trans, Math Phys Eng Sci 376(2112):20170182. https://doi.org/10.1098/rsta.2017.0182

Mansfield ML, Douglas JF (2008) Transport properties of wormlike chains with applications to double helical DNA and carbon nanotubes. Macromolecules 41(14):5412– 5421. https://doi.org/10.1021/ma702837v

Melo, R., Paz, J. (1995). Física y Química de la Madera. Volume 1. Dirección de Docencia, Universidad de Concepción.

Morais FP, Bértolo RAC, Curto JMR, et al (2019) Comparative characterization of eucalyptus fibers and softwood fibers for tissue papers applications. Materials Letters: X 4:100028. https://doi.org/10.1016/j.mlblux.2019.100028

Muraleedharan MN, Zouraris D, Karantonis A, et al (2018) Effect of lignin fractions isolated from different biomass sources on cellulose oxidation by fungal lytic polysaccharide monooxygenases. Biotechnol Biofuels 11:296. https://doi.org/10.1186/s13068-018-1294-6

Murali Krishnan J, Deshpande Abhijit P, Sunil Kumar PB (2010) Rheology of complex fluids. Springer, New York, NY

Nechyporchuk O, Belgacem MN, Pignon F (2016) Current progress in rheology of cellulose nanofibril suspensions. Biomacromolecules 17:2311–2320. https://doi.org/10.1021/acs.biomac.6b00668

Oliaei E, Lindström T, Berglund LA (2021) Sustainable development of hot-pressed all-lignocellulose composites-comparing wood fibers and nanofibers. Polymers (Basel) 13:2747. https://doi.org/10.3390/polym13162747

Pandey KK (1999) A study of chemical structure of soft and hardwood and wood polymers by FTIR spectroscopy. J Appl Polym Sci 71(12):1969–1975. https://doi.org/10.1002/(SICI)1097-4628(19990321)71:12%3c1969::AID-APP6%3e3.0.CO;2-D

Qin Y, Qiu X, Zhu JY (2016) Understanding longitudinal wood fiber ultra-structure for producing cellulose nanofibrils using disk milling with diluted acid prehydrolysis. Sci Rep 6:35602. https://doi.org/10.1038/srep35602

Rencoret J, Gutiérrez A, del Río JC (2007) Lipid and lignin composition of woods from different eucalypt species. Holzforschung 61:165–174. https://doi.org/10.1515/hf.2007.030

Rojo E, Peresin MS, Sampson WW, Hoeger IC, Vartiainen J, Laine J, Rojas OJ (2015) Comprehensive elucidation of the effect of residual lignin on the physical, barrier, mechanical and surface properties of nanocellulose films. Green Chem 17(3):1853–1866. https://doi.org/10.1039/C4GC02398F

Saarinen, T., Lille, M., & Seppälä, J. (2009) Technical aspects on rheological characterization of microfibrillar cellulose water suspensions. Annu Trans Nord Rheol Soc, 17, 121-128.

Segal L, Creely JJ, Martin AE Jr, Conrad CM (1959a) An empirical method for estimating the degree of crystallinity of native cellulose using the X-ray diffractometer. Text Res J 29:786–794. https://doi.org/10.1177/004051755902901003

Sixta H (ed) (2008) Handbook of pulp. Wiley-VCH Verlag

Stark NM, Yelle DJ, Agarwal UP (2016) Techniques for Characterizing Lignin. En: Lignin in Polymer Composites. Elsevier, pp 49–66

Stelte W, Sanadi AR (2009) Preparation and characterization of cellulose nanofibers from two commercial hardwood and softwood pulps. Ind Eng Chem Res 48:11211–11219. https://doi.org/10.1021/ie9011672

Tanaka R, Saito T, Hondo H, Isogai A (2015) Influence of flexibility and dimensions of nanocelluloses on the flow properties of their aqueous dispersions. Biomacromol 16(7):2127–2131. https://doi.org/10.1021/acs.biomac.5b00539

Tarasov D, Leitch M, Fatehi P (2018) Lignin-carbohydrate complexes: properties, applications, analyses, and methods of extraction: a review. Biotechnol Biofuels 11:269. https://doi.org/10.1186/s13068-018-1262-1

Wang H, Zhang X, Jiang Z, et al (2015) A comparison study on the preparation of nanocellulose fibrils from fibers and parenchymal cells in bamboo (Phyllostachys pubescens). Ind Crops Prod 71:80–88. https://doi.org/10.1016/j.indcrop.2015.03.086

Yang H, Yan R, Chen H, et al (2007) Characteristics of hemicellulose, cellulose and lignin pyrolysis. Fuel (Lond) 86:1781–1788. https://doi.org/10.1016/j.fuel.2006.12.013

Zhang X, Zhang L, Fan Y, Wang Z (2022) The case-dependent lignin role in lignocellulose nanofibers preparation and functional application-A review. Green energy environ. https://doi.org/10.1016/j.gee.2022.09.008

Zimmermann T, Pöhler E, Geiger T (2004) Cellulose fibrils for polymer reinforcement. Adv Eng Mater 6:754–761. https://doi.org/10.1002/adem.200400097